



On the Factors Influencing the High Stretch–Flangeability of a Low-Density 1180 MPa Fe–Mn–Al–C–Nb δ -QP Steel

Dan-Dan Cui¹ · Peng Chen¹ · Peng-Fei Wang² · Xiao-Wu Li^{1,2}

Received: 13 November 2023 / Revised: 19 December 2023 / Accepted: 25 December 2023 / Published online: 3 April 2024
© The Chinese Society for Metals (CSM) and Springer-Verlag GmbH Germany, part of Springer Nature 2024

Abstract

Low-density δ -quenching and partitioning (δ -QP) steels with excellent strength and ductility have been recently developed. However, there are still rare reports on the formability of δ -QP steels, which are critical for satisfying the manufacture of structural parts during the application in automotive industry. In the present work, an 1180 MPa Fe–Mn–Al–C–Nb δ -QP steel with a high ductility was adopted for the stretch–flangeability study. The δ -QP steel was developed by separated quenching and partitioning processes. A good hole expansion ratio (HER) of $34.9 \pm 0.9\%$ was obtained in the quenched steel, but it has been further increased to 52.2% by the tempering treatment. The improved stretch–flangeability was attributed to the enhanced austenite stability and deformation uniformity. On the one hand, the stability of austenite was increased by carbon partitioning during tempering, which reduced crack possibility via the suppression of the fresh martensite formation. On the other hand, the tempering treatment released the internal stress caused by martensitic transformation and reduced the difference in strength among different phases, resulting in an increase in the resistance to crack initiation and propagation.

Keywords Hole expansion ratio · Low-density δ -quenching and partitioning (δ -QP) steel · Stretch–flangeability · Austenite stability · Deformation uniformity

1 Introduction

Driven by the urgent requirements of increasing automobile fuel efficiency and decreasing greenhouse gases emission, lightweight has become a research hotspot in automobile industry [1]. As reported [2], 10% reduction in vehicle weight could decrease the fuel consumption of 5.5% and correspondingly lower the CO₂ emission. The application of low-density high-strength steels is one of effective methods for the lightweight of automotive sectors [3]. As a candidate

of third-generation advanced high-strength steels (AHSS), quenching and partitioning (QP) steel has attracted extensive attentions due to its excellent strength and plasticity. Speer et al. [4] took the lead in proposing the novel QP process, which involves heating to a full or partial austenitization temperature, then quenching to a temperature between martensite start (M_s) and martensite finish temperatures (M_f) to obtain an appropriate martensite and austenite fraction, followed by partitioning at or above the initial quenching temperature to make the carbon diffuse from supersaturated martensite to retained austenite (RA) [5]. Thus, the quenching temperature is a key factor for the final microstructure and mechanical properties of the QP steel.

However, the uniform and accurate temperature is not easily controlled during the actual production process, especially for large-scale or complex-shape products. For solving this problem, a novel heat treatment of quenching–tempering and partitioning (Q-T&P) was proposed, and the quenching temperature was designed as room temperature [6]. The adoption of Q-T&P can not only simplify the production process, but also expand the application scope. The δ -QP steel was then developed on the basis of the Q-T&P process, and the yield strength could be significantly improved

Available online at <http://link.springer.com/journal/40195>.

✉ Peng Chen
chenpeng@mail.neu.edu.cn

✉ Xiao-Wu Li
xwli@mail.neu.edu.cn

¹ Department of Materials Physics and Chemistry, School of Materials Science and Engineering, and Key Laboratory for Anisotropy and Texture of Materials (Ministry of Education), Northeastern University, Shenyang 110819, China

² State Key Laboratory of Rolling and Automation, Northeastern University, Shenyang 110819, China

via the carbon trapping by dislocations in ferrite during the tempering process [7]. Even though the δ -QP steel exhibits excellent tensile properties, the good formability is also required for satisfying the manufacture of structural parts [8]. However, the investigation on the formability of δ -QP steel is rarely reported so far.

The formability of steel sheets involves deep-drawing ability, stretch–flangeability, bending ability and so on [9]. Among them, the stretch–flangeability is a quite critical property to avoid fracture during forming process of actual parts [10–12]. The hole expansion capacity (HEC) is a key indicator to assess stretch–flangeability, which is obtained by hole expansion test (HET) [10]. Therefore, the stretch–flangeability of δ -QP steel was studied by HET in this work, mainly focusing on the relevant mechanism of formability.

2 Experimental

The chemical composition of the steel was Fe-2.8Mn-3.65Al-0.395C-0.037Nb (wt%). The cast ingot was reheated to 1200 °C for 3 h and hot-rolled to a sheet with the thickness of 4 mm, followed by furnace cooling after holding at 650 °C for 0.5 h. The hot-rolled sheet was then cold-rolled to 1.5-mm thick. Afterward, the Q-T&P heat treatment was adopted, which involves intercritical annealing at 795 °C for 5 min, then water quenching to room temperature (RT) (M_f is below RT), followed by partitioning at 350 °C for 5 min.

The quenched and tempered samples are designated as “DQ” and “QP”, respectively.

Uniaxial tensile tests were conducted on dog-bone-shaped samples with a gauge length of 25 mm and a gauge width of 6.25 mm at room temperature and a strain rate of 10^{-3} s^{-1} . The tensile test was performed on an Ag-Xplus250 kN machine equipped with an Epsilon extensometer, and each test was repeated for 3 times. The HET was carried out on the samples fabricated with a dimension of 84 mm \times 84 mm \times 1.5 mm, followed by piercing a hole with the diameter of 10 mm in the center, with a punching speed of 5 mm min^{-1} and a blank holder force of 40 kN (Fig. 1). After HET, the hole expansion ratio (HER) was calculated to evaluate the stretch–flangeability of the studied δ -QP steel using the following equation:

$$\text{HER} = (d_f - d_0) / d_0 \quad (1)$$

where d_0 is the initial diameter of the hole (10 mm) and d_f is the diameter of the expanded hole as far as the first through-thickness crack is observed.

The X-ray diffraction (XRD) measurement was performed on a Rigaku D/Max-2400 detector using $\text{Co-K}\alpha$ radiation. XRD samples were prepared by mechanical grinding and then electro-polishing in order to remove the surface stress layer. Electro-polishing was conducted at room temperature using 8% perchloric acid and 92% alcohol solution at an operating voltage of 20 V. The diffraction covered 2θ from 40° to 104° with a step size of 0.02°

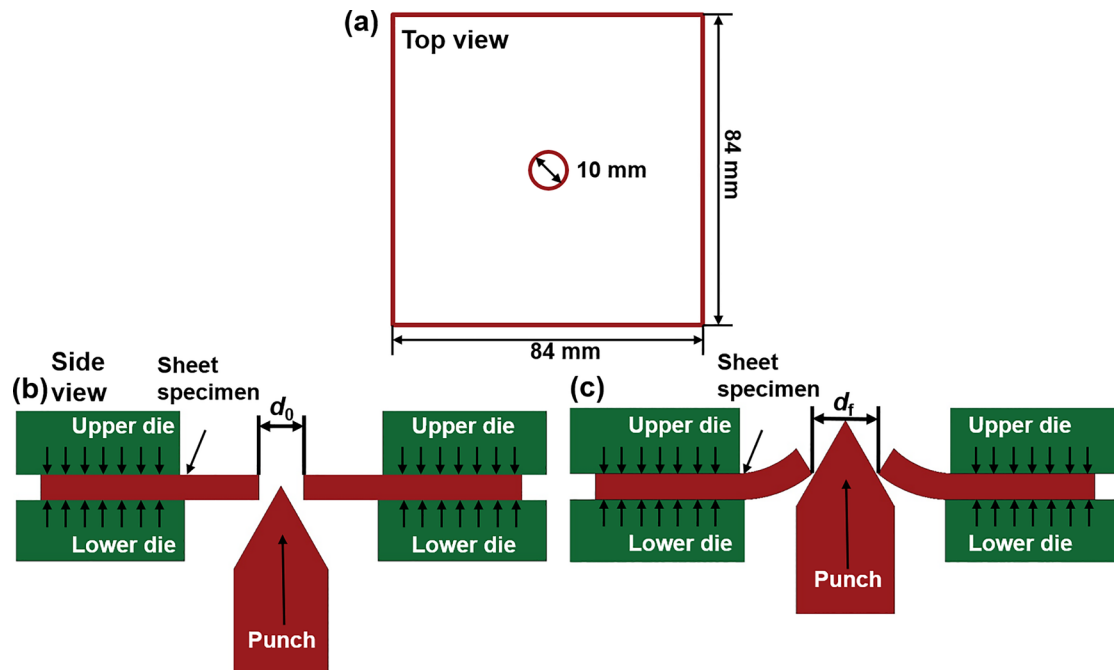


Fig. 1 Dimension of the hole expanding specimen **a**, and the schematic diagram before **b** and after **c** hole expansion test

s^{-1} , and the data were subjected to Rietveld analysis. The volume fraction (V_γ) and carbon content (C_γ) of retained austenite were calculated according to the XRD measurement. The formula for the calculation of V_γ is as follows:

$$V_\gamma = 1.4I_\gamma / (1.4I_\gamma + I_\alpha) \quad (2)$$

where I_γ and I_α are the average integrated intensities of the diffraction peaks of austenite and ferrite, respectively. The C_γ was calculated by following equation [13]:

$$C_\gamma = (\alpha_\gamma - 3.547) / 0.046 \quad (3)$$

$$\alpha_\gamma = \frac{\lambda \sqrt{h^2 + k^2 + l^2}}{2 \sin \theta} \quad (4)$$

where α_γ is the lattice parameter of austenite (in Angstrom), C_γ represents the mass fraction of carbon (in weight percentage), λ is the wavelength of X-rays, θ is the diffraction angle, and h , k and l are the lattice constants of $(200)_\gamma$, $(220)_\gamma$ and $(311)_\gamma$ peaks [14], respectively.

After standard mechanical grinding and polishing, the samples for microstructural observations were etched in 4% nital for 13 s. The high-resolution observations were performed using a scanning electron microscope (SEM, Zeiss Gemini 300) equipped with a field emission electron probe microanalyzer operated at 20 kV accelerating voltage. Electron back-scatter diffraction (EBSD) samples were prepared in the same way as XRD samples. The EBSD (OXFORD) system was attached to a SEM, and the measurements were performed at 20 kV with a scanning step of 0.08 μm . The data were processed by channel 5 software. The kernel average misorientation (KAM) maps and band contrast (BC) maps were obtained from EBSD results.

3 Results

The representative microstructures of the samples DQ and QP were characterized by SEM, as shown in Fig. 2. Both microstructures consist of martensite/austenite (M/A) island and ferrite. A duplex metallurgical structure of austenite and ferrite was obtained during the intercritical annealing at 795 $^\circ\text{C}$, and the partial austenite was transformed into martensite during the following cooling process. Subsequently, the tempering of sample QP promoted the carbon partitioning from supersaturated martensite to retained austenite. Thus, the fraction of retained austenite in two samples is nearly the same, and they are 25.2 vol.% and 25.6 vol.% for the samples DQ and QP, respectively, according to the XRD results in Fig. 3a, and more carbon was enriched in the austenite of the sample QP than that of the sample DQ. The carbon content in austenite was 1.80 wt% and 2.03 wt% for the samples DQ and QP, respectively, as estimated by Eq. (3).

The engineering stress–strain curves of the samples DQ and QP are shown in Fig. 3b, and the corresponding data of mechanical properties are listed in Table 1. Both samples exhibit a high tensile strength (above 1180 MPa) and a relatively high elongation (above 18%), which are comparable to or even better than the commercial QP1180 products [15, 16]. A higher yield strength was obtained in the sample QP rather than the sample DQ, owing to the carbon trapping by dislocations in ferrite during tempering [7]. The samples QP and DQ show good tensile elongations of $26.8 \pm 0.8\%$ and $19.9 \pm 0.3\%$, respectively. The higher ductility and obvious necking of the sample QP should be attributed to the enhanced deformation uniformity by tempering, which can partially release the internal stress [17]. Besides, the ductility of martensite in the sample QP was also improved by the

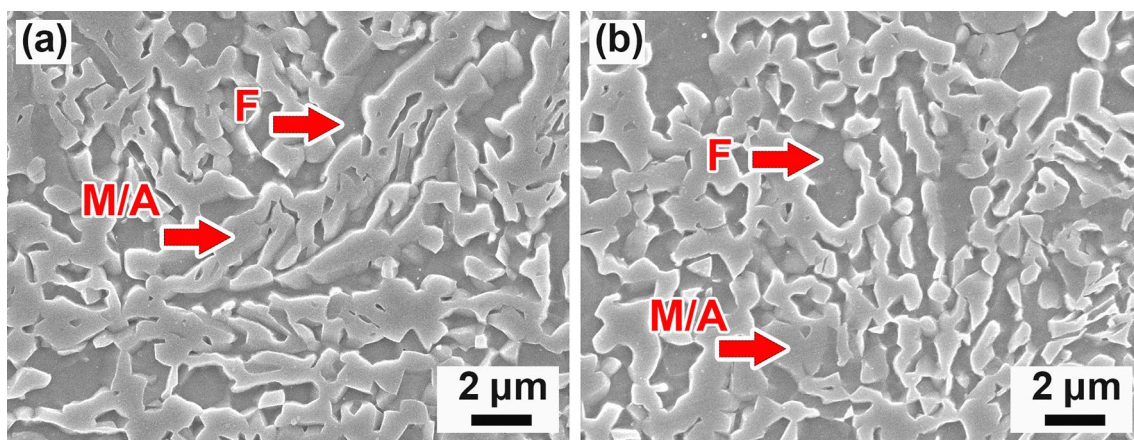


Fig. 2 SEM images of the microstructures in the samples DQ a and QP b

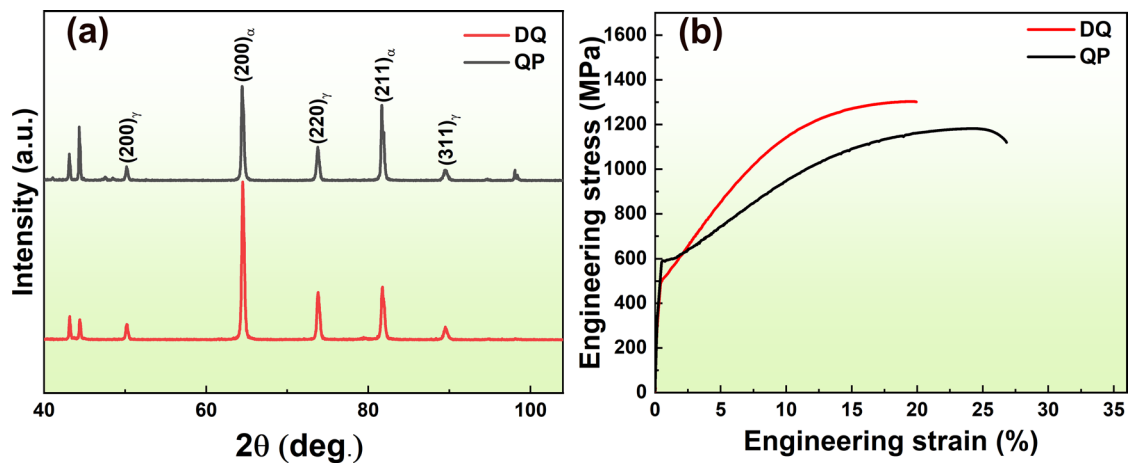


Fig. 3 X-ray diffraction patterns **a** and tensile engineering stress–strain curves **b** of the samples DQ and QP

Table 1 Experimental date of uniaxial tensile and hole expansion properties of the samples QP, DQ and referenced QP1180

Samples	YS (MPa)	UTS (MPa)	TE (%)	PSE (GPa%)	HER
DQ	509.8 ± 10.9	1303.1 ± 6.7	19.9 ± 0.3	26.0	34.9 ± 0.9
QP	598.5 ± 6.8	1181.7 ± 14.0	26.8 ± 0.8	31.7	52.2 ± 0.2
QP1180 [15]	1015	1165	13.2	15.4	28.0

YS, UTS, TE, PSE represent the yield strength, ultimate tensile strength, total elongation and product of strength and elongation, respectively

emission of carbon during tempering; it is also beneficial for the better ductility.

The stretch–flangeability of studied steels was evaluated using HET, and the HER is calculated and listed in Table 1, where the HER of commercial QP1180 was also included for comparison. Both samples exhibit an excellent stretch–flangeability, reflected from the higher HER compared with QP1180 steel reported in some previous work [10, 15, 18, 19]. A higher HER ($52.2 \pm 0.2\%$) was achieved in the sample QP than that ($34.9 \pm 0.9\%$) in the sample DQ, so that the sample QP has a better ability to resist edge fracture during complex-shape forming [8]. Such a nearly 50% increase in HER should be closely related to the increased stability of austenite and enhanced mechanical properties [20].

4 Discussion

4.1 Effect of Austenite Stability

The austenite fractions near the fracture were measured by XRD and EBSD, and the measuring positions are indicated in Fig. 4a–c. Larger amounts of austenite were consumed during the hole expansion process (Fig. 4d, f), indicating that the TRIP effect plays a significant role in the

stretch–flangeability of the studied steels [21]. The initial fraction of austenite in two samples is similar (Fig. 4d), but the carbon content in austenite is different, resulting in the diverse chemical stabilities [20]. The expansion-hole process involves punching and expanding. On the one hand, some fresh martensite was formed on the punched surface, which would induce the occurrence of cracks due to the high brittleness of martensite [22]. Due to a lower stability of austenite in the sample DQ, more fresh martensite might be formed during punching. On the other hand, the deformation induced martensitic transformation also happened during the expansion, which has been verified by the reduced austenite fraction near the fracture (Fig. 4d). The big difference in hardness between formed martensite and ferrite would easily lead to the initiation of cracks. At the edge of punched hole (0 mm distance from hole), more austenite was consumed for the formation of martensite in the sample DQ (Fig. 4d).

In view of a larger HER for the sample QP, there actually exists a larger strain at the same position away from the expanded hole. Specifically, at the position 0 and 5 mm from the hole along radial direction, the macro-strains are 0.53 and 0.055 for the sample DQ, respectively, but 0.62 and 0.087 for the sample QP, based on the results of hole expanding simulation (Fig. 5). The closer to the hole, the less of the austenite fraction is (Fig. 4d). It is clear that the retained austenite fraction at all positions in the sample QP

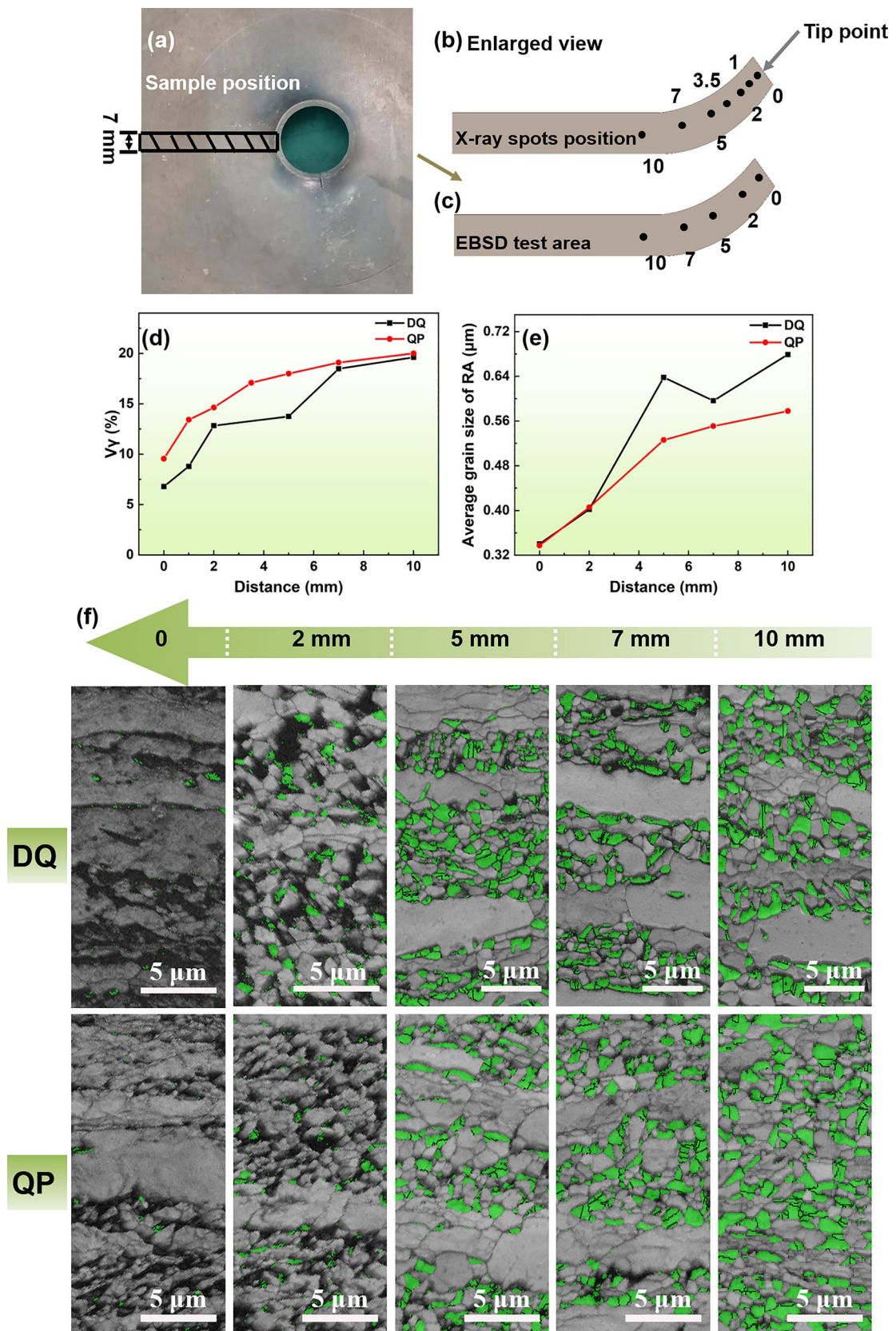


Fig. 4 Measuring positions of hole expanding samples **a–c** (unit: mm); **d** volume fraction of austenite as a function of distance from the fracture based on the XRD results; **e** average grain size of RA as a function of distance from the fracture based on the EBSD results; **f** band contrast and phase distribution maps at different measuring positions. Note that the green color represents austenite

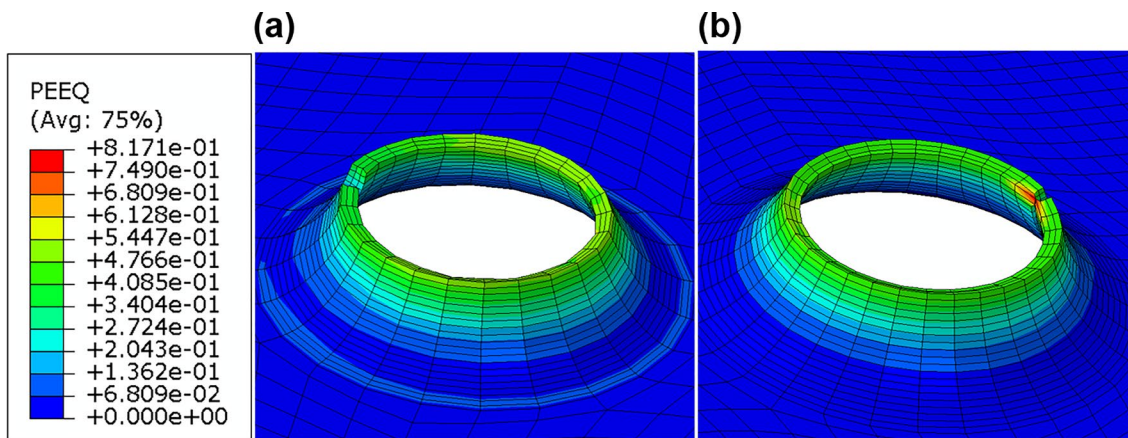


Fig. 5 Macroscale simulation of the HET process for the samples DQ **a** and QP **b**

is higher than that in the sample DQ in spite of a larger strain, as a result of a higher stability of retained austenite in the sample QP. With the strain increasing to 0.62, the austenite fraction is decreased from 0.20 to 0.095 in the sample QP, while the austenite fraction in the sample DQ is reduced from 0.20 to 0.068 with the increase in strain. Even though there are 0.068 and 0.095 austenite retaining at the hole edge in the samples DQ and QP, respectively, only very small amount of austenite can be observed in the phase maps due to a limited resolution of EBSD measurements (Fig. 4d, f) [19]. Therefore, the improved austenite stability in the sample QP by tempering is quite beneficial for a larger HER and thus for a better stretch–flangeability (Table 1).

Furthermore, the evolution of austenite grain size with strain was traced by EBSD measurements (Fig. 4e). The austenite grain size was gradually refined with the increase in strain. Yoon et al. [23] have reported that blocky austenite was transformed firstly during the deformation process due to a lower mechanical stability [24]. The austenite with a

larger size was consumed at low strain, which further refined the austenite grain and thus enhanced the austenite stability; for example, at the 2-mm position, the austenite grain sizes of the sample DQ and QP were refined to 0.40 and 0.41 μm , respectively (Fig. 4e,f).

4.2 Effect of Deformation Uniformity

Figure 6 shows the microstructure near the fracture of these two samples. The cracks can be often detected in the deformation microstructure of two samples with an initial mixed microstructure of M/A and ferrite. In addition to cracking in ferrite matrix (mode I) or through M/A (mode II), most of cracks were formed at the interfaces between M/A and ferrite (mode III). With the progress in expanding of studied steels, the dislocations piled up at such interfaces, which acted as obstacles for the dislocation motion and thereby created local strain concentration [17, 25]. Moreover, the strength difference between M/A and ferrite would result in

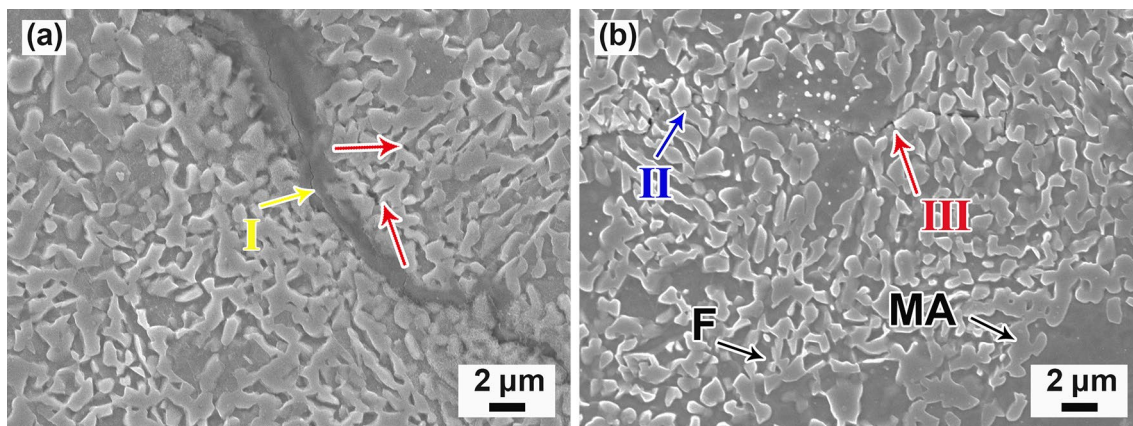


Fig. 6 Microstructures near the fracture of the samples DQ **a** and QP **b** after HET. Note that F and MA represent ferrite and martensite/austenite

the strain partitioning, and thus in an inhomogeneous local strain during expanding process. KAM maps confirmed the higher density of dislocations accumulated at interfaces (Figs. 7 and 8). The cracks were easily nucleated at the interface between M/A and ferrite when the local strain was high enough for the interface decohesion, as marked by III red arrows in Fig. 6 [25]. After the cracks were formed at the interface, they propagated along the interface or into the soft phase of ferrite, as indicated by the yellow arrow in

Fig. 6. Apart from the interface decohesion, the M/A island became instantaneously fractured as the internal stress at the M/A has reached its fracture stress, so that a small number of cracks were also observable in the M/A. Considering the formation mechanism of three types of cracks during expanding, the better stretch–flangeability of the sample QP is closely related to the crack initiation and propagation resistance. On the one hand, the tempering process partially releases the internal stress [26] generated by martensitic

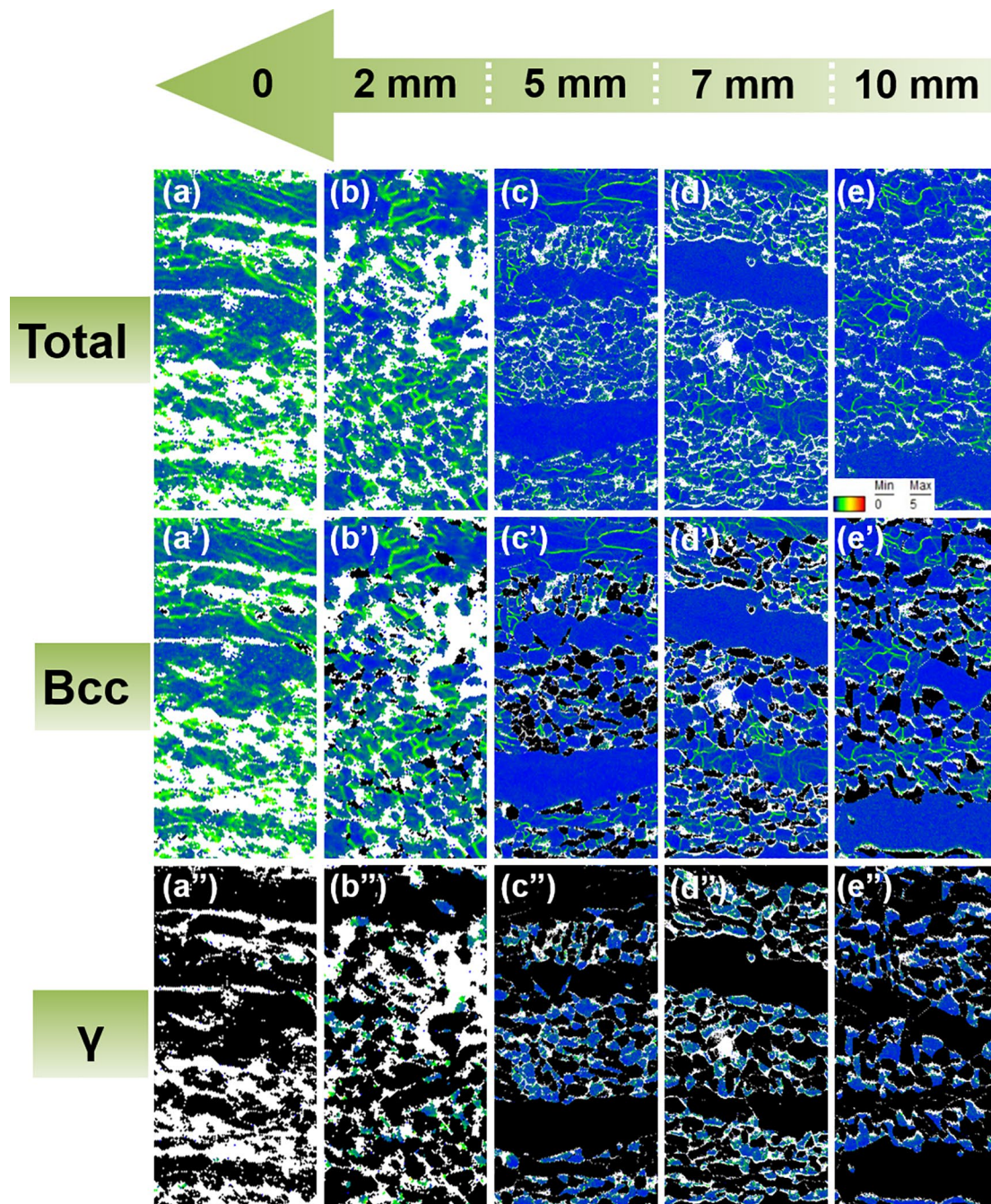


Fig. 7 KAM images of the sample DQ at different measuring positions: a–e total, a'–e' bcc, and a''–e'' austenite

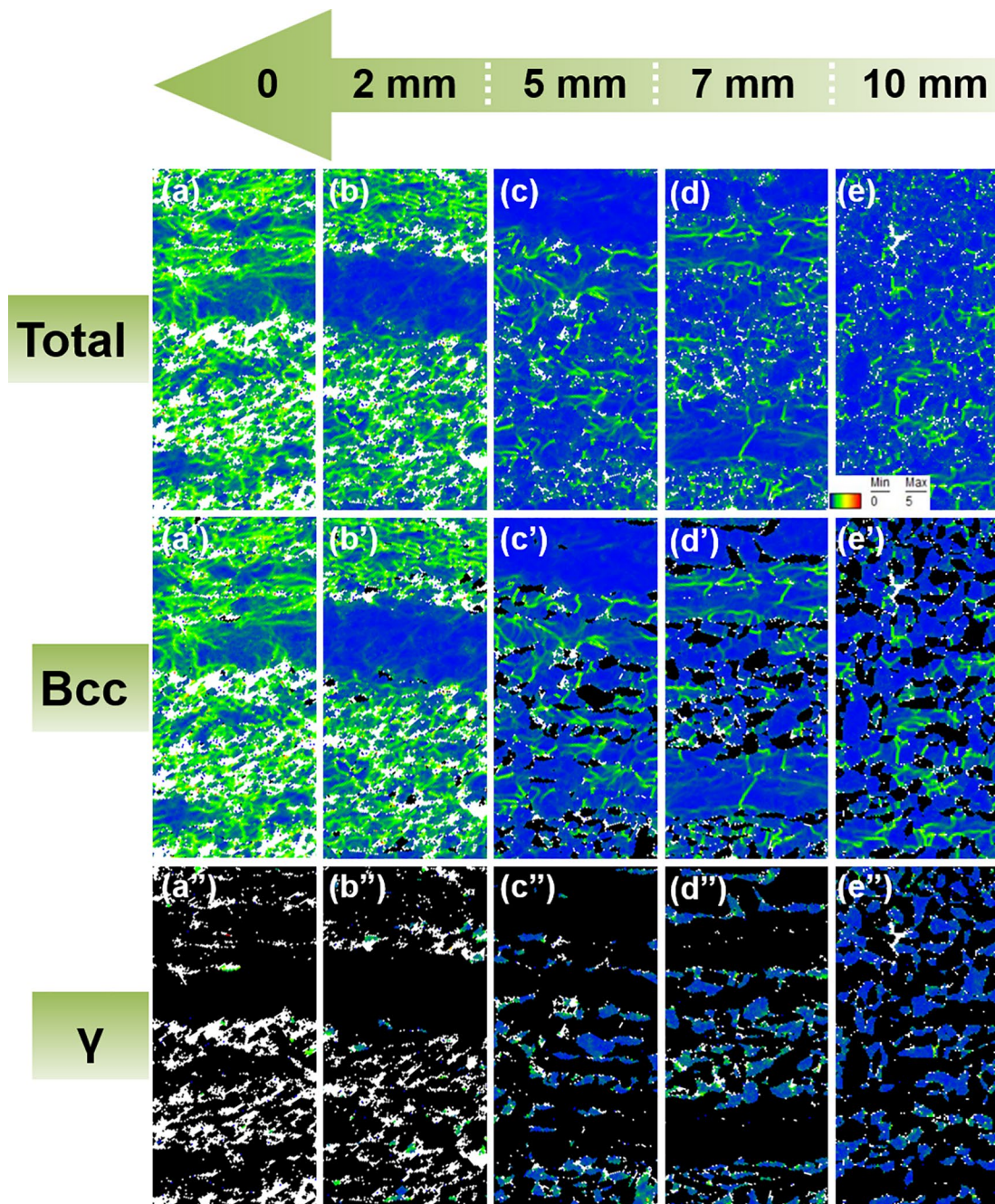


Fig. 8 KAM images of the sample QP at different measuring positions: a–e total, a'–e' bcc, and a''–e'' austenite

transformation during quenching [27], which increased the crack resistance. On the other hand, the hardness of martensite was reduced by tempering and thus enhanced the deformation uniformity among three phases [28]. Specifically, the hardness of ferrite and M/A in the sample QP is 271 ± 15.87 HV and 306 ± 17.08 HV, respectively, but 283 ± 18.51 HV and 345 ± 14.79 HV in the sample DQ. That is to say, a less hardness difference was obtained in the sample QP rather than DQ. This significantly contributed to

a better stretch–flangeability of the sample QP, due to the predominant crack initiation at the interfaces. In addition, high-density dislocations near the ferrite interface in the sample QP were introduced by martensitic transformation during the quenching process. The carbon was trapped by dislocations, which would strengthen the ferrite interface. This is propitious to delay the MA/ferrite interface cracking and thus to achieve a good stretch–flangeability in the sample QP.

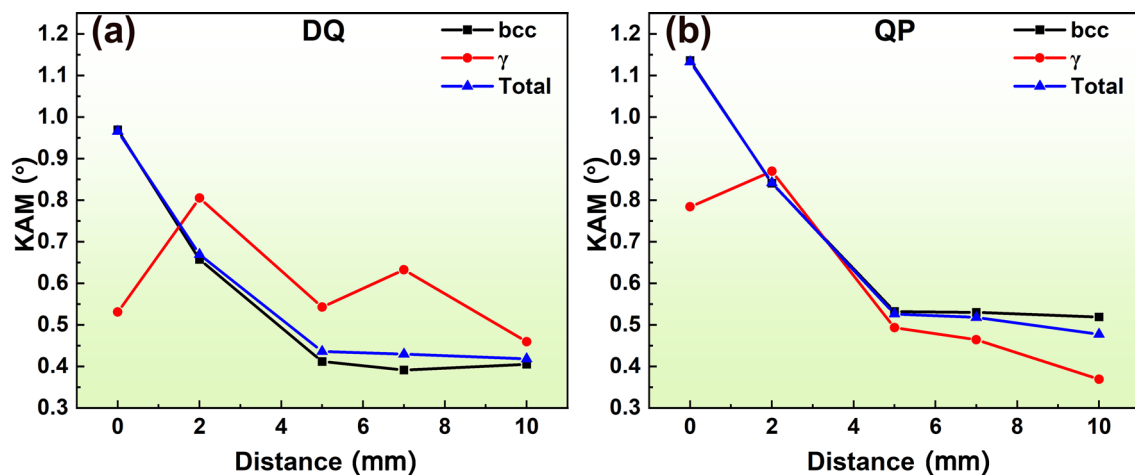


Fig. 9 Variation of KAM value with the distance from the hole of the samples DQ **a** and QP **b** after HET

Considering the noteworthy effect of deformation uniformity on the stretch–flangeability, the KAM maps of two expanded samples were analyzed (Figs. 7 and 8). The KAM values in austenite and the other phases, including ferrite and partial martensite with a body-centered cubic (bcc) structure, were obtained according to EBSD results, and partial martensite with high distortion is hard to be detected by EBSD. The KAM values are proportional to the density of geometrically necessary dislocations (GNDs), which are closely related to plastic deformation [29]. It is clear that the KAM values increased as the position was close to the hole owing to the raised strain and exhibited a more uniformly distributed GNDs were presented in the sample QP rather than DQ (Figs. 5 and 9). At lower strain level, both samples exhibited less GNDs (Figs. 7e and 8e). The higher density of GNDs in austenite of the sample DQ is attributed to the internal stress generated by martensitic transformation during cooling, which was released by tempering (Fig. 9a). Thus, the austenite of the sample QP has a lower KAM value (Fig. 9b). With the increase in strain, the difference in KAM value between austenite and the other phases became larger in the sample DQ, but very small in the sample QP, especially at distances of 2–5 mm from the hole (Fig. 9). At the high strain position of 0-mm distance, more strain has partitioned in the soft phase, inducing a decrease in the KAM value of austenite, as reported by our previous work that more strain was undertaken by the soft phase of matrix [30]. At this position, the difference in KAM value in the samples of DQ and QP is 0.44 and 0.35, respectively. Besides the decreased strain difference, the martensite ductility and the austenite strength were also increased through the carbon partitioning during tempering. Consequently, the increased deformation uniformity by tempering significantly raised

the crack resistance and therefore brought about a better stretch–flangeability.

5 Conclusions

A low-density 1180 MPa δ -QP steel has been investigated in this study, focusing on the influencing factors on the high stretch–flangeability. The tensile properties and hole expansion ratio have been tested, and the microstructure evolution has been carefully characterized. The main conclusions can be summarized as follows:

1. Both quenched and tempered samples exhibit a high tensile strength above 1180 MPa and an elongation larger than 18%, which are comparable or even better than the commercial QP1180 products. Especially, a better stretch–flangeability has been obtained in the tempered sample; the HER increases greatly from $34.9 \pm 0.9\%$ of the sample DQ to $52.2 \pm 0.2\%$ of the sample QP.
2. The enhanced austenite stability by tempering contributes to a higher HER. The improved TRIP effect in the sample QP postponed the formation of fresh martensite; it is beneficial for the suppression of cracking caused by the highly brittle fresh martensite. Moreover, the deformation uniformity during hole expanding can be raised by tempering, thus enhancing the crack resistance at interfaces.

Acknowledgements This work was supported by the National Natural Science Foundation of China (Grant Nos. 52171108 and 51804072) and the Fundamental Research Funds for the Central University (Grant Nos. N2202007 and N2202011). Special thanks are also due to the instrumental or data analysis from Analytical and Testing Center, Northeastern University, China.

Declarations

Conflict of interest The authors state that there are no conflicts of interest to disclose.

References

- [1] W. Zhang, J. Xu, *Mater. Des.* **221**, 110994 (2022)
- [2] J. Galan, L. Samek, P. Verleysen, K. Verbeken, Y. Houbaert, *Rev. Metal. Madrid*. **48**, 125 (2012)
- [3] Y.F. Pu, F.W. Ma, J.Y. Zhang, M. Yang, *IEEE Access*. **6**, 8596 (2018)
- [4] J. Speer, D.K. Matlock, B.C. De Cooman, J.G. Schroth, *Acta Mater.* **51**, 2616 (2003)
- [5] D.Q. Zou, S.H. Li, Ji. He, *Mater. Sci. Eng. A* **680**, 60 (2017)
- [6] H.L. Yi, P. Chen, Z.Y. Hou, N. Hong, H.L. Cai, Y.B. Xu, D. Wu, G.D. Wang, *Scr. Mater.* **68**, 373 (2013)
- [7] P. Chen, G.D. Wang, A.V. Ceguerra, A.J. Breen, S.P. Ringer, X.C. Xiong, Q. Lu, J.F. Wang, H.L. Yi, *Metall. Mater. Trans. A* **49**, 238 (2017)
- [8] J.I. Yoon, J. Jung, J.G. Kim, S.S. Sohn, S. Lee, H.S. Kim, *J. Mater. Sci.* **52**, 7816 (2017)
- [9] M. Mukherjee, S. Tiwari, B. Bhattacharya, *Int. J. Min. Met. Mater.* **25**, 210 (2018)
- [10] X. Chen, H. Jiang, Z. Cui, C. Lian, C. Lu, *Proced. Eng.* **81**, 720 (2014)
- [11] D. Casellas, A. Lara, D. Frómata, D. Gutiérrez, S. Molas, L. Pérez, J. Rehr, C. Suppan, *Metall. Mater. Trans. A* **48**, 90 (2016)
- [12] S.K. Paul, *Materialia* **9**, 100566 (2020)
- [13] E. Jimenez-Melero, N.H. van Dijk, L. Zhao, J. Sietsma, S.E. Offerman, J.P. Wright, S. van der Zwaag, *Acta Mater.* **55**, 6718 (2007)
- [14] S. Yan, X. Liu, W.J. Liu, T. Liang, B. Zhang, L.Z. Liu, Z. Yang, *Mater. Sci. Eng. A* **684**, 267 (2017)
- [15] K.S. Diao, H.M. Jiang, L. Wang, X.P. Chen, 2012 China automotive lightweight technology seminar. Beijing. (2012).
- [16] Baosteel's new ultra-high strength steel products are launched in the world, machinist metal forming. **7**, 2 (2015). <https://go.exlibris.link/q0CZ9yLF>.
- [17] P. Chen, X.W. Li, P.F. Wang, G.D. Wang, J.Y. Guo, R.D. Liu, H.L. Yi, *J. Mater. Res. Technol.* **17**, 1340 (2022)
- [18] Y. Wang, Y. Xu, Y. Wang, J. Zhang, C. Guo, X. Wang, W.Z. Zhao, H.L. Liu, *J. Mater. Res. Technol.* **26**, 5512 (2023)
- [19] Y.R. Im, E.Y. Kim, T. Song, J.S. Lee, D.W. Suh, *ISIJ Int.* **61**, 576 (2021)
- [20] X. Xu, B.Y. Xu, P. Chen, R.D. Liu, G.D. Wang, H.L. Yi, *Mater. Today Commun.* **24**, 101034 (2020)
- [21] R.M. Wu, W. Li, C.L. Wang, Y. Xiao, L. Wang, X.J. Jin, *Acta Metall. Sin. -Engl. Lett.* **28**, 386 (2015)
- [22] S.H. Sun, A.M. Zhao, R. Ding, X.G. Li, *Acta Metall. Sin. -Engl. Lett.* **31**, 220 (2018)
- [23] J.I. Yoon, J. Jung, H.H. Lee, G.S. Kim, H.S. Kim, *Met. Mater. Int.* **22**, 1011 (2016)
- [24] F. Zhao, P. Chen, B. Xu, Q. Yu, R.D.K. Misra, G.D. Wang, H.L. Yi, *Mater. Charact.* **179**, 111327 (2021)
- [25] P. Chen, J. Fu, X. Xu, C. Lin, H.L. Yi, *J. Mater. Sci. Technol.* **87**, 55 (2021)
- [26] K. Zhang, P. Liu, W. Li, Z.H. Guo, *Acta Metall. Sin. -Engl. Lett.* **28**, 1268 (2015)
- [27] P. Chen, Dissertation, Northeastern University, 2017.
- [28] M. Azuma, S. Goutianos, N. Hansen, G. Winther, X. Huang, *Mater. Sci. Technol. -Lond.* **28**, 1097 (2012)
- [29] C.S. Han, H. Gao, Y. Huang, W.D. Nix, *J. Mech. Phys. Solids* **53**, 1198 (2005)
- [30] P. Chen, R. Chen, X.W. Li, *Mater. Charact.* **189**, 111954 (2022)

Springer Nature or its licensor (e.g. a society or other partner) holds exclusive rights to this article under a publishing agreement with the author(s) or other rightsholder(s); author self-archiving of the accepted manuscript version of this article is solely governed by the terms of such publishing agreement and applicable law.